Arising from: Mendoza-Halliday, Major et al. *Nature Neuroscience* https://doi.org/10.1038/s41593-023-01554-7 (2024).

This **supplement** provides additional, in-depth explanation of points raised in the main text, as well as a more complete set of references.

1. vFLIP does not find more sites with a significant fit than FLIP when an appropriate threshold is used

The Paper[1] does not state the threshold it used for vFLIP (the only threshold noted is .265 for FLIP), thus we sought to estimate an appropriate threshold for vFLIP to examine the performance of this algorithm. Because vFLIP runs FLIP many times iterating over different possible frequency ranges, there are a large number of multiple comparisons that we must take into account when determining the threshold for vFLIP. We estimated the threshold for vFLIP that was statistically equivalent to the .265 used for FLIP to appropriately compare the performance of vFLIP to FLIP. Accordingly, we first ran FLIP 10,000 times on randomly generated pink noise (10,000 simulations of 30 channels with 1000 timepoints and 75 trials of 1/f noise). We then passed this noise through the code that accompanied *The Paper*, which first uses Fieldtrip™ to generate the spectrolaminar pattern for this noise, then uses FLIP to determine if there was the "X" shaped pattern across channels for low and high frequency power. Across the 10,000 simulations, the .265 threshold of FLIP corresponded to a false positive rate (detection of the "X" pattern in noise) of approximately 2.3%, this corresponded to an estimated false discovery rate of less than 5% in the public dataset accompanying The Paper.

To determine the threshold for vFLIP, we repeated this same estimation procedure 500 times (fewer simulations were used for vFLIP because vFLIP is computationally intensive and slow to run). The vFLIP threshold that gave the same false positive rate as FLIP was .76. Using this threshold on the shared data that accompanies *The Paper*, vFLIP detects 3% fewer penetrations as having the "X" pattern than FLIP, rather than 17% more (as reported in *The Paper*). Therefore, the threshold used in *The Paper* was one that likely had a high false positive rate. Similar results were seen for FLIP and vFLIP in the new dataset reported in this *Matters Arising* work, where 64% of penetrations were detected by FLIP at a .265 threshold and 61% were detected by vFLIP at a .76 threshold.

2. vFLIP tends towards very narrow frequency range selections in an overly broad parameter space.

First, vFLIP's relatively unrestricted search of the frequency band space usually results in selection of narrow (~10 Hz) frequency bands, indicating that vFLIP operates in a parameter space with numerous potential peaks and power gradient crossing points, many of which are likely spurious (see main text **Fig. 2**).

Second, while allowance for some variation in peak alpha-beta and gamma frequencies is a strength of vFLIP analysis, *"low" frequencies are allowed vary from 1-70 Hz, and "high" frequencies can vary from 30-150 Hz,* resulting in frequency selections that often deviate from an alpha/beta-gamma motif (**Fig S-1**).

Notably, there are numerous cases where the "low" frequencies extend into the gamma band, and high

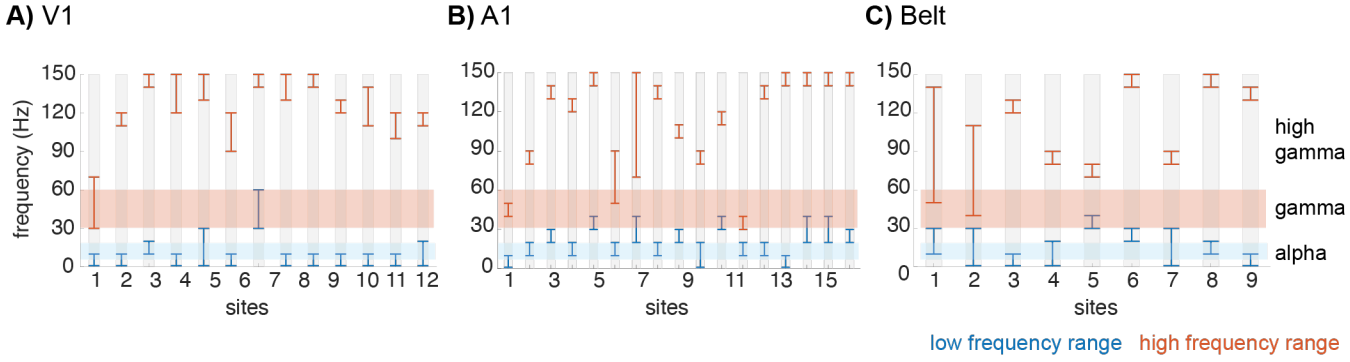

Fig S-1 - Automatically selected frequency bands from the vFLIP algorithm for each site in **A)** V1, **B)** A1, and **C)** Belt. "High" frequencies are orange, "low" frequencies are blue, and alpha/beta, gamma, and high gamma ranges are color-coded accordingly.

frequencies extend well beyond the conventional gamma band of 30-60 Hz and into the 120-150 Hz high gamma band, that is likely representative of spiking rather than oscillatory activity. In fact, ***there are only a few cases in which the low/high frequencies are in the alpha-beta and gamma ranges respectively***, contrary to *The Paper*'s suggestion. Because vFLIP labels any "low" frequency as "alpha/beta," and the authors don't

report what frequencies vFLIP selected, it's unclear if the alpha/beta-gamma motif reported in the paper is actually gamma-high gamma, delta-gamma, etc.

3. False positive rate of spatially imprecise LFP measures for FLIP and image similarity analysis. Key measures used in *The Paper* produce increasing false positive rates as the spatial resolution of the measure decreases. Critically, the thresholds used in *The Paper* are only appropriate when spatial resolution is high and are not adjusted for the lower spatial resolution of LFP measures using a distant reference. This leaves unclear what is the true, quantifiable percentage of laminar motifs that have the X-like pattern that the authors call "ubiquitous."

The SSIM image similarity metric used in *The Paper* to establish the similarity of spectrolaminar motifs suffers from reduced specificity with increased spatial blur. **Fig S-2A** shows the image similarity using SSIM for random noise with increasing blur. The image similarity rapidly increases even for random noise as the image is blurred more. **Fig S-2B** shows an example of two spectrolaminar plots taken from *The Paper*'s dataset that, even with opposite motifs, achieve an image similarity of .45, higher than the similarity for any of the within or across species comparisons in Figure 8i of *The Paper*.

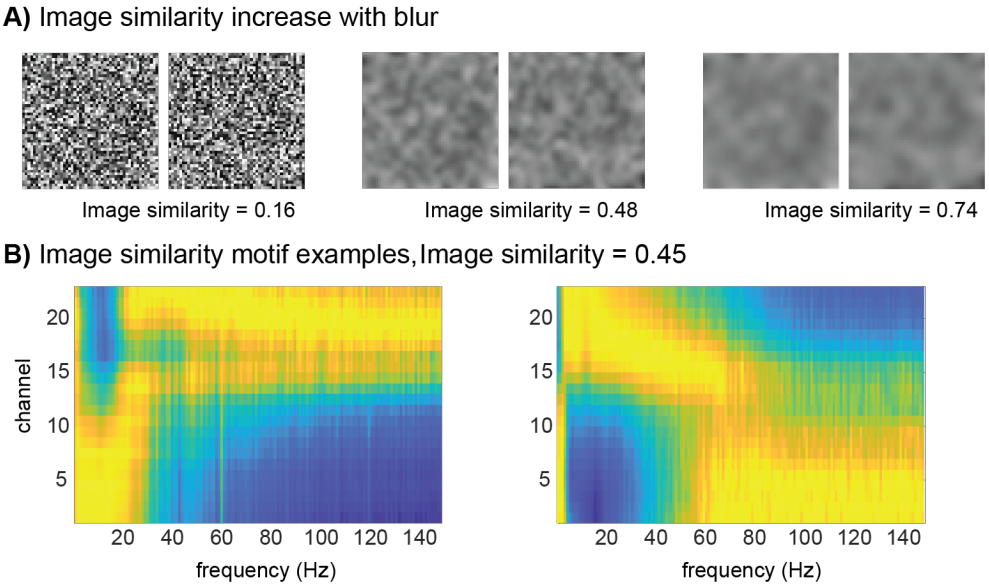

Fig S-2. Interpretability of the Image Similarity measure. **A)** Image similarity increases for the same examples of noisy images with increasing blur. Using SSIM the similarity between random noise images was calculated with increasing blur. The image similarity values below the examples in this panel reflect the average image similarity of 10000 pairs of random images unblurred and then blurred at 2 different amounts. **B)** Image similarity for relative power in two examples probes from the publicly available datasets from *The Paper*. These two probes were chosen as having strong positive and negative G. Despite the notable differences and near inverted profiles, the image similarity reaches a value of 0.45, which is higher than the similarity for within and across species comparisons reported in *The Paper* (figure 8i).

This is not a flaw in the SSIM method, rather the SSIM method is an inappropriate measure for determining if two spectrolaminar patterns match. SSIM was developed to evaluate whether a compressed picture would be judged similarly to the original by a human observer. It thus examines factors like local contrast, luminance, and structure and incorporates Weber's law[2]. Therefore, for example, noise with greater blur does look more similar by eye even if the underlying data are not similar at all. For assessing the similarity of spectrolaminar patterns, however, this is not an appropriate measure. A measure such as mean squared error, or a non-parametric measure, might be appropriate.

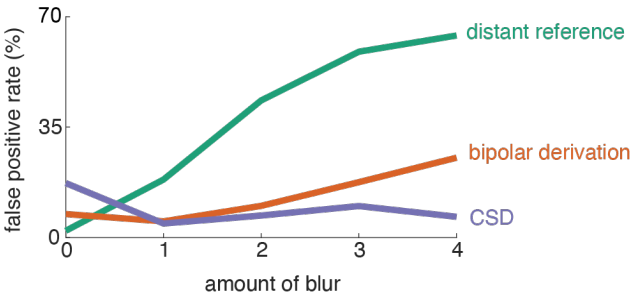

Fig S-3 evaluates the effects of volume conduction by implementing simulations to estimate the false positive rate as a factor of spatial resolution at the .265

Fig S-3 Increase in false positive rates for FLIP as a function of blur (volume conduction). Each point reflects 10,000 simulations of 30 channels with 1000 timepoints (simulating 1 second of data sampled at 1000 Hz) and 75 trials of 1/f pink noise (no patterns should be detected as these are random patterns) at each datapoint convolved with a 1-d blurring kernel to approximate volume conduction in the channel direction. For a distant reference, the false positive rate increases to over 60% with increasing blur. Bipolar referencing reduces the increase in false positives and Laplacian re-referencing keeps the false positive rate below 10% across these levels of blur.

threshold that is used in *The Paper* for distant referencing, in comparison to bipolar and CSD derivations. Note that as spatial resolution decreases, false positive rate for the distant reference function increases rapidly. The same functions for bipolar and CSD derivations remain flat.

4. Additional Broad Concerns:

4.1. Conflation of oscillatory with sensory-evoked activity. *The Paper* attributes the reported motif to a laminar organization of alpha and gamma oscillations [3,4]. Despite the focus on oscillatory activity, *the Paper* does not explicitly isolate oscillations from evoked responses. As described in *The Paper*, normalized relative power is calculated based on the -0.5 to 0.5 s interval around the onset of a stimulus. As such, the estimated relative power change does not distinguish between oscillations and evoked responses[5–8]. **Fig S-4A** depicts LFP spectrograms and power spectra in three channels in the supragranular, granular, and infragranular layer (2, 6, and 12, respectively) from *The Paper*'s publicly shared data sets.

For the low frequencies, power was normalized to the mean in the -1 to 1 s interval, and for the high frequencies, power was normalized to the -1 to -0.25 s interval before stimulus onset. Evidently, the onset of the stimulus (indicated by the dashed line) is followed by a broad band high-frequency response in the gamma/BHA-band, as well as a low-frequency stimulus-evoked responses at 3 to 6 Hz. However, sustained ***gamma-range oscillations*** are not observed in any of the channels, which undermines claims about "oscillations," and poses problems for subsequent work seeking to model the motif using gamma-specific mechanisms. The pre-stimulus period shows high power in the 15 to 20 Hz band, which is conventionally termed the beta-band. ***Alpha oscillations*** (8 – 12 Hz) appear to be absent in the recording. The spectrograms show a strong overlap between channels, indicating volume conduction due the distant reference of the LFP. **Fig S-4B** depicts the Current Source Density (CSD) power spectra and demonstrates that the broadband response appears to be strongest in the supragranular layers, while the pre-stimulus beta activity is strongest in the granular layers. Stimulus-evoked and beta-band activity are attenuated in the infragranular channels.

In sum, the spectral analyses show that the spectrolaminar motif does not account for a contamination of oscillatory dynamics by evoked responses, and that the presence of ongoing oscillations in the alpha- and gamma-bands is not established. Numerous dedicated methods have been proposed that resolve oscillatory contributions to brain operations by: 1) identifying individual/local peak frequencies actually present in the data rather than blindly averaging over predefined bands[9], 2) implementing tools to separate rhythmic and non-rhythmic contributions[10,11], 3) eliminating spurious oscillatory activity due to harmonics and non-sinusoidal properties[12,13], 4) characterizing transient burst events[14], and 5) parametrizing cycle-by-cycle dynamics[15,16]. In general, traditional spectral methods used without such controls do not provide an accurate picture of underlying oscillatory dynamics[11].

4.2. Conflation of Broadband High frequency Activity (BHA) with band-limited (30-60 Hz) gamma. Band-limited gamma oscillations (30 – 60 Hz) have been linked to coordinated interaction of pyramidal neurons and inhibitory interneurons[17,18]. Short bursts of activity in the higher 70-150 Hz range known as "high gamma" [19,20] or "broadband high frequency activity" (BHA) [21,22], contains a mixture of ripple (90-130 Hz) frequencies along with more wideband, transient (non-oscillatory) activity. BHA has further been shown to correlate strongly with multiunit activity [19,21–23], while band-limited gamma oscillations are associated with irregular firing patterns, also [24]. Moreover, gamma oscillations and BHA have been shown to play distinct roles in perception and cognition [25,26]. Due to the differences in the underlying mechanisms of gamma oscillations and BHA it is crucial to study these activities in isolation.

4.3. Inadequate consideration of the "State of the art" established by prior work. Contrary to statements in the Introduction of *The Paper*, at least 12 papers have analyzed laminar activity profiles across *multiple* cortical areas in monkeys [5,27–37] and in humans[38]. Interestingly, the Halgren paper[38] proposes a cortical feedback role for alpha operating as a traveling wave through pyramidal neuron connections in the supragranular layers, which is a distinctly different mechanism from that advocated by *The Paper*. Bollimunta et al [39] utilize two terms that could be helpful here: (1) alpha generator, which refers to the active transmembrane current flow region,

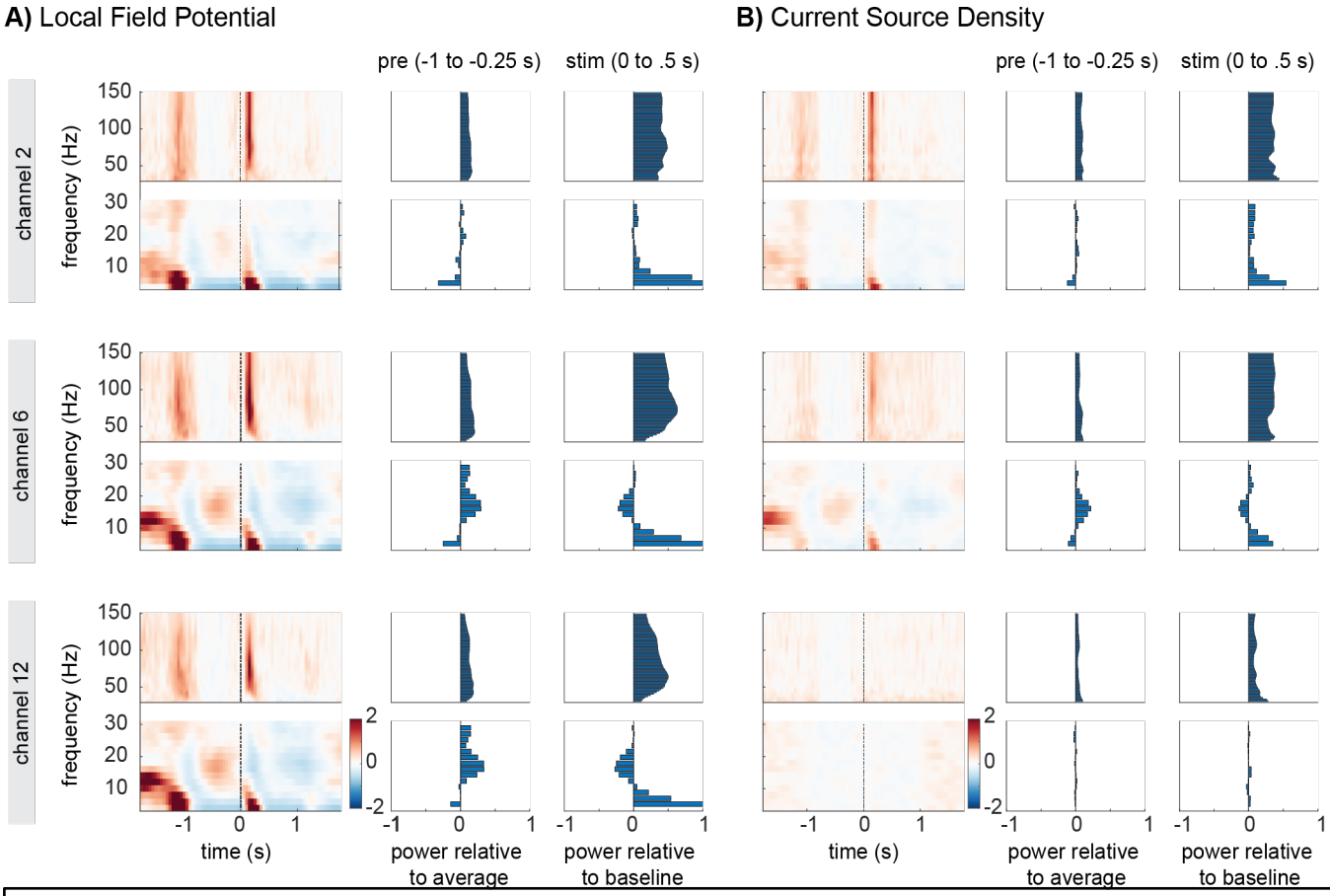

Fig S-4 Oscillatory dynamics in the gamma- and alpha-bands are not established in *The Paper*. Spectrograms and spectra of the LFP, **A**) and Current Source Density (CSD, **B**) for three channels in the supragranular (2), granular (6), and infragranular layers (12), recorded from ventrolateral prefrontal cortex (vlPFC; publicly shared data from *The Paper*). Spectrograms are shown for the -1.75 to 1.75 s interval, with the stimulus onset at 0 seconds (dashed line). The spectra were calculated by averaging over the -1 to 0.25 s and 0 to 0.5 s intervals. For the low frequencies, power was normalized to the average power at each frequency in the channel, and for the high frequencies, power was normalized to the baseline intervals. **A)** The high-frequency spectrogram in the LFP demonstrates a broadband evoked response at 50 – 150 Hz following the onset of the stimulus. The evoked potential is indexed by the power increase in the 0 to 10 Hz band. The stimulus evoked activity is present in all trials, albeit strongest in the supragranular channel 2. The stimulus is preceded by high power in the beta-band (15-20 Hz) that is visible in all channels, but strongest in channel 6 and 12. **B)** CSD calculated from the LFP. Stimulus-evoked responses in both high and low-frequency ranges appear strongest in the supragranular channel 2. The pre-stimulus beta-band activity is strongest in the granular layer and disappears in the deep layers.

and (2) alpha pacemaker, which is the alpha generator that drives the other alpha generators. Though the generators appear in superficial (largest), middle and deep layers [37], the alpha pacemaker is in the deep layers in V2 and V4. Another important methodological point evident from prior studies is that CSD profiles must be analyzed on a single-case basis. Averaging across CSD profiles from different penetrations requires that the laminar profiles be perfectly aligned, which is rarely possible. Thus, averaging destroys information, produces circumscribed artifacts and yields physiologically implausible CSD profiles (see Fig 7 and Extended Fig 7). Findings from the earlier papers cited above, along with the large number of laminar recording studies focusing on single visual [40–46], somatosensory [37,47–50], auditory [6,30,36,51–66] and motor/prefrontal areas [67–70] collectively comprise a broader State-of-the-Art context in which to evaluate new ideas about cortex-wide motifs.

4.4. Ambiguous anatomical reconstructions. *The Paper* provides single examples of histological sections from several cortical areas to illustrate methods by which key physiological findings (e.g., “gamma power peak” and laminar power function crossing points) are localized to specific layers in the cortex. Each example is followed by drawings that illustrate summary interpretations presumably based on viewing of the entire set of histological section from all penetrations and lesions. Several concerns arise from this presentation.

The broadest concern is that in chronic recording studies, a penetration by an electrode like those used here usually leaves a prominent glial scar[31,44,71], and such scars are not apparent at the sites that *The*

Paper represents as the electrode's position (white circles mark probe channels) in Fig. 4a,b and Extended Data Fig. 4 in *The Paper*. Possible electrode scars are sometimes visible (e.g., Extended data Fig 4b) but not at the site and angle of the indicated probe location. The absence of a clear glial scar marking the electrode track suggests that the section used for illustration is not at the center of the electrolytical lesion, however, the reader cannot evaluate the quality, position and extent of lesions, as the critical adjacent sections are not provided. As such, the histology provides anecdotal rather than unequivocal evidence for laminar localization of key physiological features. A more quantitative supplementary presentation of all sections showing evidence of lesions and electrode tracks could alleviate this concern.

Specific concerns arise from the illustrations The Paper presents: **1)** *Lesions indicating the depth of the alpha/beta power peak in V1 and PMD are in the white matter*. As *The Paper* itself notes, this may be due to volume conduction from proximal areas. This localization deviates from the proposed motif, but it also underscores the risks (see **3.** above) inherent to the relatively poor spatial specificity of the LFP. **2)** *Most of the five areas used for histological verification deviate in some way from the proposed motif* (Fig 4 and Extended data Figs 3 and 4). In LPFC, only 3-4/10 cases (30-40%) indicate power gradient crossings in L4. In PMD, the gamma power peak is depicted in L4 and the crossover is depicted in L5/6. In MST only 1 of the 2 cases provided depicts a power gradient crossing that is arguably in L4.

5. Physiologically realistic models to support laminar electrophysiology

To explain the inconsistencies between the laminar CSD and LFP profiles, the authors refer to previous computational work featuring a Neural Mass Model (NMM) that was developed based on a previously reported spectrolaminar motif in frontal cortex[3]. The NMM consists of two built-in alpha and gamma oscillators, constrained to produce band-limited dynamics at 10 and 40 Hz, respectively. However, neither the data presented in *The Paper*, nor in the referenced publication show band-limited peaks at 10 or 40 Hz (see above). While the NMM publication uses these band-limited frequencies to calculate the relative power gradient, FLIP and vFLIP select a wide range of frequencies to calculate the relative power for the slow and fast frequencies (see above). The model further relies on the assumption that the slow and fast oscillations are each generated by one single pyramidal population. However, *in vivo*, pyramidal populations exist across all layers and generate a wide range of frequencies. Similarly, model synaptic input and return currents are located at the apical tuft and basal dendrites, whereas in biology these currents can be spread throughout the dendritic tree [72]. Overall, the discrepancies between the NMM and the data indicate that the NMM may be ineffective at localizing the generators of the transmembrane currents responsible for the observed LFP/CSD patterns.

To accurately resolve laminar origins of LFP/CSD neuronal oscillations in an unbiased manner we propose instead constructing "informed" biophysical models utilizing detailed implementations of known cortical microcircuitry, multiple populations of excitatory (pyramidal IT, PT, CT, stellate) and inhibitory interneurons (SOM, PV, VIP, NGF, etc.), arrayed in realistic laminar cortical architecture, with precisely configured synaptic connection probabilities/locations, realistic dendritic morphologies, ion channel and synaptic time constants [73,74]. Ideally also for dynamics like the alpha rhythm, models would include *thalamo*cortical circuitry[73,75]. These approaches create biophysical models that can simulate laminar LFPs/CSDs, using them to delineate population-level origin of neuronal oscillations[73,76,77]. Findings based on these approaches have demonstrated that LFP/CSD signals depend strongly on dendritic locations of synapses and show the importance of supragranular layers and inputs from other brain structures in creating alpha[76,78–80]. In the long run, these data-driven approaches will better complement empirical studies in resolving the laminar sources of neuronal dynamics including oscillations.

Table S1 – significant FLIP fits from *The Paper* are not ubiquitous

	Penetrations	# of sites with the motif	# of sites with inverse motif	No detect	% sites with the motif	% of sites with inverse motif	% no detect
STUDY 1							
PFC	79	64	4	11	81.0	5.1	13.9
V4	109	63	13	33	57.8	11.9	30.3
7A	41	37	1	3	90.2	2.4	7.3

FEF	51	14	26	11	27.5	51.0	21.6
STUDY 2							
PFC	234	59	67	108	25.2	28.6	46.2
MST	145	86	27	32	59.3	18.6	22.1
LIP	86	49	11	26	57.0	12.8	30.2
MT	112	47	40	25	42.0	35.7	22.3
total	857	419	189	249	48.9	22.1	29.1

Supplemental Table 1 – Summary of results from *The Paper.* The table indicates the number of penetrations detected by FLIP having the X-shaped "ubiquitous" motif for low and high frequency power across brain regions in the shared dataset from *The Paper*. Substantial interregional variation is seen, with as many as ~90% of sites detected in area 7A from study 1 and as few as 54% in PFC from study 2. Substantial inter-study variation is seen, e.g. 87% of PFC sites in study 1 are fit by FLIP, while only 54% are fit in study 2.